Voltage- and ligand-gated ion channels in floor plate neuroepithelia of the rat

ARTICLE *in* NEUROSCIENCE · SEPTEMBER 1998

Impact Factor: 3.36 · DOI: 10.1016/S0306-4522(97)00641-6 · Source: PubMed

Pergamon

PII: S0306-4522(97)00641-6

Neuroscience Vol. 85, No. 4, pp. 1135–1149, 1998

0306–4522/98 $19.00+0.00

VOLTAGE- AND LIGAND-GATED ION CHANNELS IN FLOOR PLATE NEUROEPITHELIA OF THE RAT

F. FRISCHKNECHT† and A. D. RANDALL*

Division of Neurobiology, MRC Laboratory of Molecular Biology, Hills Road, Cambridge CB2 2QH, U.K.

Abstract—Whole-cell patch-clamp recordings were used to characterize the membrane properties and ion channel complement of floor plate neuroepithelia in embryonic and neonatal rats. The average resting potential was close to −60 mV, the capacitance was ~7 pS and the membrane time constant averaged 31 ms, in both neonates and embryos. Two types of K^+ current were identified (i) a slowly activating, slowly inactivating current that was present in all cells, and (ii) a rapidly inactivating current that was present in 39% of cells from neonates and 64% of cells from embryos. K^+ currents were significantly larger in neonates than embryos. Na^+ currents were absent from all neuroepithelial cells examined. In contrast, the majority of floor plate cells exhibited a significant Ca^{2+} current. Biophysically this current activated at potentials positive to −60 mV and exhibited fast, voltage-dependent, inactivation. The Ca^{2+} current was equipermeant to Ca^{2+} and Ba^{2+}, sensitive to 40–120 μM Ni^{2+} and only slightly inhibited by 100 μM Cd^{2+}.

These and other observations indicated this current is mediated by low-voltage-activated (i.e. T-type) Ca^{2+} channels. The majority of floor plate cells tested also exhibited responses to the neurotransmitter GABA which produced robust inward currents at negative membrane potentials, in chloride-loaded cells. Both the pharmacology and voltage-dependence of the GABA-activated currents indicated they arose from activation of $GABA_A$ receptors. © 1998 IBRO. Published by Elsevier Science Ltd.

Key words: floor plate, electrophysiology, GABA receptors, calcium channels, potassium channels, development.

The development of the mammalian CNS is a complex process that utilizes a wide range of different intra- and intercellular signalling pathways to produce the intricate connections of the mature nervous system.[12,45] Throughout development, cells undergo many carefully controlled transitions including cell division, selective differentiation, migration, extension of processes, synaptogenesis and in some cases programmed cell death. It has become clear that certain structures form within the immature CNS in order to play a specific developmental role, and subsequently disappear soon after this role has been fulfilled. A good example of such a structure is the floor plate.[2,17,21,26,29,57,64,65]

The floor plate is a ventral mid-line neuroepithelial structure formed early in the developing CNS.[42,44,46,47] Floor plate neuroepithelia are induced by the axial mesodermal cells of the underlying notochord.[33,41–43,46,50,58] In rodents the floor plate persists into early postnatal life, eventually disappearing around postnatal day 7 (P7). This structure seems to play a variety of roles in the development of the CNS including dorsoventral patterning, motor neuron induction and guidance of the axons of commissural neurons during their passage across the mid-line.[13,16,18,21,23,25,33,57,64,65] The majority of axons receiving guidance cues from the floor plate arise from cells located in dorsal regions of the spinal cord and brain stem. Their axons project towards the floor plate and cross the ventral mid-line, thereby eventually forming axon commissures.[12,22,56] Having crossed the mid-line, most commissural axons alter their trajectory and bend longitudinally before continuing close to the midline towards their target synapses.[4,12,22,30,49,53,56,63] Mutations in zebrafish, *Xenopus* and mice that eliminate the floor plate and/or notochord produce highly abnormal axonal trajectories, not only in commissural neurons but also in certain longitudinal projections.[3,5,8,17,18]

It has been shown that floor plate cells either release, or express on their cell surface, chemoattractant/chemorepellent molecules which direct pioneering axons.[37,54,55,56] Although it is likely that many of these molecules remain as yet undiscovered, two molecular families, the netrins[9,26,48,49] and the semaphorins/collapsins,[36,37,61] clearly exhibit long range chemoattractant and/or chemorepellent

*To whom correspondence should be addressed.
†Present address: European Molecular Biology Laboratory, Meyerhofstrasse 1, Heidelberg, Germany.

Abbreviations: ACSF, artificial cerebrospinal fluid; CAM, cell adhesion molecule; E, embryonic day; EGTA, ethyleneglycolbis(aminoethylether)tetra-acetate; f_c, filter corner frequency; HEPES, *N*-2-hydroxyethylpiperazine-*N*′-2-ethanesulphonic acid; 5-HT, 5-hydroxytryptamine; HVA, high-voltage-activated; KS, Kolmogorov–Smirnoff; LJP, liquid junction potential; LVA, low-voltage-activated; NK-1, neurokinin-1; P, postnatal day; TEA, tetraethylammonium; TTX, tetrodotoxin.

activity. F-Spondin and NrCAM are two examples of cell adhesion molecules (CAMs) expressed by floor plate cells and responsible for contact-dependent guidance of commissural axons which have completed their journey to the ventral mid-line.[6,28,51,55] NrCAM seems to function by the formation of a heterophilic interaction with the axonal IgCAM axonin-1.[52] In addition, the floor plate releases sonic hedgehog, which amongst other things is strongly implied in motor neuron induction.[33,41,46]

Recent work has provided evidence for a bi-directional communication between neurons and floor plate cells. Notably, De Felipe and colleagues demonstrated substance P released from a subset of commissural axons seemingly activates neurokinin-1 (NK-1) receptors on floor plate cells, which is thought to stimulate the release of floor plate chemoattractants.[11] Activation of NK-1 receptors by substance P derivatives elevates the intracellular Ca^{2+} concentration of floor plate cells;[19] a process mediated through inositol triphosphate-generated release of Ca^{2+} from intracellular stores. It is likely that such rises in intracellular Ca^{2+} trigger chemoattractant release through a process of Ca^{2+}-dependent exocytosis.

To date analysis of floor plate function has mainly utilized the techniques of anatomy, biochemistry and both cell and molecular biology. To obtain further insights into signalling processes involving floor plate cells, we have initiated an electrophysiological study of floor plate cells in both neonatal and embryonic tissue slices. Some of this work has been previously presented in abstract form.[14]

EXPERIMENTAL PROCEDURES

Preparation of brain slices

P0 neonatal Sprague–Dawley rats (Charles River, Margate, U.K.) were killed by decapitation. The brain was removed and transferred to ice-cold gassed (95% O_2/5% CO_2) artificial cerebrospinal fluid (ACSF, for composition see below). The forebrain was removed by means of a coronal scalpel cut and the caudal aspect of the cut surface was glued to the stage of a vibraslice (Campden Instruments, Oxford, U.K.). The ventral part of the brain was placed in close apposition to a block of 2% agarose previously glued to the stage. The stage and attached tissue were immersed in ice-cold gassed ACSF and coronal slices of 300–350 μm thickness cut in a dorsoventral orientation. Slices from the brainstem region were identified and subsequently stored in a Petri dish containing gassed ACSF at room temperature.

Embryonic spinal cord slices were prepared in a similar fashion except that the entire embryo was glued head down (and surrounded on three sides by blocks of agarose) to the stage of the vibraslice. Embryonic slices were ~800 μm in thickness.

In P0 slices recordings were made from the floor plate adjacent to the aqueduct in the brainstem. In embryonic slices the recording sites were in the floor plate adjacent to the fourth ventricle of rostral aspects of the spinal cord. Both neonatal and embryonic slices remained electrophysiologically viable for up to 50 h.

Electrophysiological set-up

Cells were visualized with a modified upright microscope (Optiphot-2 from Nikon, Kingston, U.K.) equipped with long-working distance 10× and 40× water-immersion objectives and infra-red diascopic differential interference-contrast Nomarski optics. Tissue slices were individually transferred to a recording chamber mounted on the stage of the microscope. The chamber was modified from a commercially available product (Warner, New Haven, CT, U.S.A.). Slices were held in position using bent 30-gauge syringe needles attached to the walls of the chamber. The bath was continuously perfused (1–2 ml/min) via a small antechamber with gassed ACSF. All drug applications and solution changes were made via the perfusion system and were therefore applied with some delay due to the dead space in the system. We measured this delay by examining the blocking action of both tetrodotoxin (TTX, 1 μM) on the neuronal Na^+ current and tetraethylammonium (TEA, 20 mM) on neuroepithelial K^+ currents. The average delay was 150 s (data not shown), and this was accounted for in all of our subsequent analysis.

Whole-cell patch-clamp recording

Patch-clamp electrodes of 2–8 MΩ resistance were fabricated from 1.2 mm diameter thick-walled borosilicate glass capillaries (Clark Electromedical, Pangbourne, U.K.), using a standard horizontal electrode puller (Sutter Instruments, Novato, CA, U.S.A.). Electrodes were subsequently fire polished using a commercially available microforge (Narishige, London, U.K.).

Electrodes were filled with the intracellular solution of choice (see below), before being mounted onto the headstage of the recording apparatus (Axopatch 1D amplifier with CV-4 headstage, Axon Instruments, Foster City, CA, U.S.A.). The headstage in turn was mounted on the platform of a long-range piezoelectric micromanipulator (Sutter Instruments MP 300, Novato, CA, U.S.A.). Before immersing the recording electrode in the bath solution, positive pressure was applied to its tip by mouth. Under visual control, the electrode tip was then positioned close to the cell of interest. The recording electrode resistance was monitored in voltage-clamp by observing the current response to a 1 mV voltage pulse. As the electrode tip encroached upon the targeted cell an increase in the tip resistance occurred. At this time positive pressure was removed from the electrode and gentle suction applied. This usually resulted in the formation of a giga-seal of resistance >3 GΩ. Fast capacitance transients were cancelled before application of further suction and simultaneous high-voltage "zaps" (2 V d.c., 0.1 to 1 ms duration) were used to enter the whole-cell recording configuration. Whole-cell capacitance transients were then neutralized and the value of series resistance and capacitance noted. Series resistance compensation of 70–90% was applied in all recordings.

Acquisition and analysis of data

The patch-clamp amplifier was interfaced with a personal computer via a Digidata 1200 interface and the pClamp6 suite of programs (Axon Instruments, Foster City, CA, U.S.A.). Voltage protocols were generated and the resultant data waveforms recorded under control of this software. Voltage-clamp data were filtered at filter corner frequency (f_c)=2–10 kHz before digitization at two to 10 times f_c. In both current and voltage-clamp, standard recording protocols consisted of the application of a test current or voltage pulse every 10 s. In voltage-clamp recordings, leak subtraction was performed with a standard negative going P-over-4 protocol. Both leak-subtracted and non-leak subtracted data were stored to disk.

Data were analysed using the Clampfit program (Axon Instruments, Foster City, CA, U.S.A.) with support from the spreadsheet QuattroPro (Borland, Scotts Valley, CA,

U.S.A.) and the graphing and fitting routines of SigmaPlot (Jandel Scientific, Erkrath, Germany). Resting Ohmic input impedances were measured from non-leak subtracted data by calculating the slope conductance between −90 and −70 mV. Activation curves were fit with a standard Boltzmann curve of the form

$$G/G_{max}=1/(1+\exp(-(V_t-V_{1/2})/k))$$

where G is conductance, V_t the test potential, $V_{1/2}$ the potential for 50% activation and k the Boltzmann slope factor. Inactivation curves were fit with the related relationship

$$G/G_{max}=h\infty=1/(1+\exp((V_t-V_{1/2})/k))$$

Unless otherwise stated all data are presented as mean ± S.E.M. Statistical testing was carried out using two-tailed *t*-tests, Mann–Whitney *U*-tests or the large sample approximation of the Kolmogorov–Smirnoff test (KS-test).

Solutions for electrophysiology

All solutions were made from analytical grade salts using double distilled de-ionized water. Osmolarity was measured by freezing point depression.

All extracellular solutions were based upon a standard ACSF. The basic solution consisted of (mM): NaCl, 124; $NaHCO_3$, 26; NaH_2PO_4, 1.5; KCl, 3; $CaCl_2$, 2; $MgCl_2$, 1; D-glucose, 10. The solution was equilibrated with 5% CO_2/95% O_2 generating a pH of 7.3–7.4. For recordings made using 2–10 mM extracellular Ba^{2+}, the $CaCl_2$ of the standard ACSF was exchanged for $BaCl_2$ at the required concentration. For solutions requiring elevated $CaCl_2$, or the inclusion of TEACl, $LaCl_3$, $CdCl_2$, $NiCl_2$, EGTA or TTX the appropriate salt was simply added to the ACSF. Particular care was taken to saturate the ACSF solution with O_2/CO_2 before adding Ba^{2+} salts which were otherwise prone to precipitation.

Three electrode solutions were utilized in this study, the first was designed as an ersatz intracellular milieu and will be referred to as ICS1, its contents were (mM) KCH_3SO_4, 110; NaCl, 10; HEPES–KOH, 35; EGTA, 5; $MgCl_2$, 5; ATP, 2; GTP, 0.2, pH 7.3, 295 mOsm. The second electrode solution, referred to as ICS2, was used to eliminate K^+ currents to aid the isolation of Ca^{2+} conductances. ICS2 consisted of (mM) $CsCH_3SO_4$, 108; NaCl, 10; HEPES–CsOH, 24; EGTA, 9; $MgCl_2$, 4.5; ATP, 4; GTP, 0.3, pH 7.3, 295 mOsm. The third electrode solution, ICS3 consisted of (mM) CsCl, 110; HEPES–CsOH, 35; NaCl, 10; $MgCl_2$, 5; EGTA, 5; ATP, 2; GTP, 0.2, pH 7.3, 295 mOsm and was used to load cells with Cl^- ions in order to facilitate the detection of GABA-mediated Cl^- currents at negative holding potentials.

Potentials stated in the text have not been corrected for the following liquid junction potentials (LJPs): in standard extracellular ACSF ICS1 (+9.1 mV), ICS2 (+9.9 mV) and ICS3 (+3.4 mV), in ACSF supplemented with 20 mM TEACl and 10 mM $BaCl_2$ ICS2 (+10.9 mV). To calculate the true membrane voltage, these LJP values should be subtracted from any stated potential.

RESULTS

Although the floor plate performs the majority of its known developmental duties in intermediate embryonic life, its presence can be detected immunologically well into the first week of postnatal life.[19,28] In this study we investigated the membrane properties of floor plate neuroepithelia in tissue slices derived from both day of birth rat pups and embryonic day (E)15 rat embryos. Confirmation that our recording sites were located within the floor plate came from post-experimental immunostaining for the NK-1 receptor, a well-documented floor plate marker. The data described herein comes from a total of 358 electrophysiological recordings from neonatal floor plate cells in the brainstem and 48 recordings from floor plate cells in the embryonic spinal cord.

Basic membrane properties of floor plate epithelial cells

In solutions designed to mimic the physiological situation (extracellular ACSF and intracellular ICS1, see Experimental Procedures), the average resting potential of 161 non-neuronal floor plate cells, determined in current-clamp recordings, was −58.9 ± 1.0 mV (Fig. 1A). In further current-clamp experiments, the injection of hyperpolarizing current pulses into neonatal floor plate cells caused a passive charging of the membrane with a time constant of 31 ± 12 ms (Fig. 1B, top). Membrane charging of the opposite polarity was observed with small depolarizing current injections. Somewhat larger depolarizing injections of current, in contrast, caused the activation of a significant hyperpolarizing conductance. This was manifested in two ways, firstly as a sag observed in the voltage trace at sufficiently advanced levels of depolarization (Fig. 1B, asterisk) and secondly in a faster discharging of the membrane upon the removal of the current injection pulse (Fig. 1B, arrow). This latter observation indicates the presence of a depolarization-induced increase in membrane conductance (i.e. channel opening). No evidence for either conventional Na^+− or Ca^{2+}-dependent action potentials was ever found.

Having characterized the basic membrane properties of floor plate cells, we next used conventional voltage-clamp techniques to analyse the classes of voltage-dependent ion channel present in these cells. In voltage-clamp the mean somatic capacitance of neonatal floor plate cells was measured as 7.4 ± 0.3 pF (n=232, Fig. 2C), indicating that floor plate cells are of quite modest size (i.e. 8–15 μm). Floor plate cells derived from embryonic tissue exhibited a similar capacitance 7.0 ± 1.0 pF.

In addition to the rapidly charging somatic capacitance component, the large majority of cells usually possessed a small slowly charging capacitance component, that we were never able to completely neutralize with the appropriate circuitry of the patch-clamp amplifier (data not shown). This indicates that the membrane of floor plate cells does not behave as a simple single electrical compartment but possesses some more electrically distal elements, presumably arising from short processes (see also Refs 6 and 62).

Under the approximately physiological conditions described above, the resting input impedance of neonatal floor plate cells was 610 ± 120 MΩ (n=24), corresponding to a resting membrane conductance of the order of 2.2 pS/μm^2, a value similar to that found

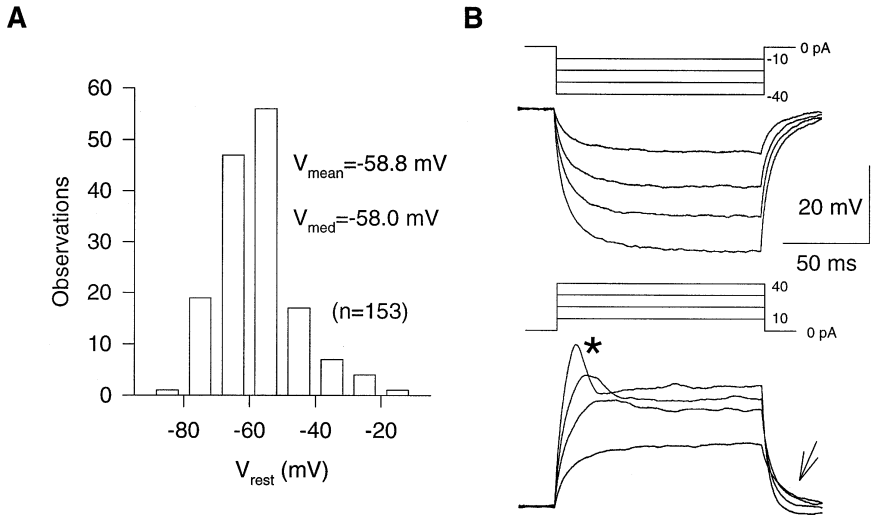

Fig. 1. Basic membrane properties of non-neuronal cells of the floor plate. (A) A frequency histogram of the resting membrane potential of 161 floor plate neuroepithelia; the mean and median values of the membrane potential are indicated. (B) Examples of responses to hyperpolarizing (top) and depolarizing (bottom) current injections (10–40 pA) applied to a single floor plate cell recorded in current-clamp mode. The larger depolarizing current injections activate a significant repolarizing conductance that is manifested as the downwards sag in the voltage responses (asterisk, bottom). The average resting membrane potential of this cell was -56 mV. The arrow indicates the faster recovery to resting potentials observed upon termination of depolarizing current injections of sufficient amplitude to activate the repolarizing conductance.

for many central neurons.[20] The average resting input impedance increased to 2.5 ± 0.4 GΩ (n=17) when an electrode solution (ICS2) containing Cs^+ instead of K^+ was used, a significant difference (P<0.01, KS-test). This, and the observation that intracellular dialysis with Cs^+ depolarized the zero current potential (data not shown), indicate that the resting potential of floor plate neuroepithelia is mainly determined by K^+ conductances.

Potassium currents in floor plate neuroepithelia

In voltage-clamp experiments in which neonatal floor plate cells were depolarized with series of incrementally large voltage steps, from a holding potential of -80 mV, slowly-activating ($\tau = 5.4 \pm 1.1$ ms at V_t=+50 mV) slowly-inactivating outward currents were seen in 37 out of 61 cells (e.g., Fig. 2A). The remaining neonatal cells (24 out of 61, 39%), additionally possessed a more transient outward current component, as illustrated by the exemplar recording shown in Fig. 2B.

Recordings from embryonic floor plate cells revealed a similar situation, with some cells containing only very slowly-inactivating outward currents (Fig. 2C), and some cells containing both rapidly-inactivating and very slowly-inactivating outward currents (Fig. 2D). In contrast to neonates, the floor plate cells expressing a significant transient outward current formed the majority in embryos (14 of 22 cells, 64%).

Evidence that both the rapidly-inactivating and slowly-inactivating outward current components arose from K^+ channel activation was provided by their practical elimination in the presence of intracellular Cs^+. In recordings made with ICS1, both current components were also significantly depressed by extracellular application of the K^+ channel blocker TEACl (20 mM); although the sustained component of the response was somewhat more sensitive to this agent (data not shown).

The transient inward current indicated by the arrows in Fig. 2C and D is a T-type Ca^{2+} current, whose properties are more fully described below. In the absence of K^+ current inhibition, this inward current was much more difficult to detect in neonates (see Fig. 3A for an example). Under a variety of recording conditions, we found no evidence in either neonates or embryos, for currents pharmacologically or biophysically resembling the fast TTX-sensitive neuronal Na^+ current. This is in agreement with the finding that floor plate cells were not competent to fire action potentials in current-clamp experiments (Fig. 1B).

We were interested to see if we could find any further differences between the floor plate cells which expressed the transient outward K^+ current and those which solely expressed the sustained delayed-rectifier like current. Our analysis revealed that although the resting membrane potentials [-57.6 ± 2.5 mV (without transient current, n=30) vs -59.6 ± 3.1 mV (with transient current, n=25)] and membrane capacitances [7.1 ± 0.5 pF (without transient current, n=37) vs 9.1 ± 1.0 pF (with transient current, n=26)] were not significantly different (Mann–Whitney U-test), the resting input impedance was greater (P<0.05,

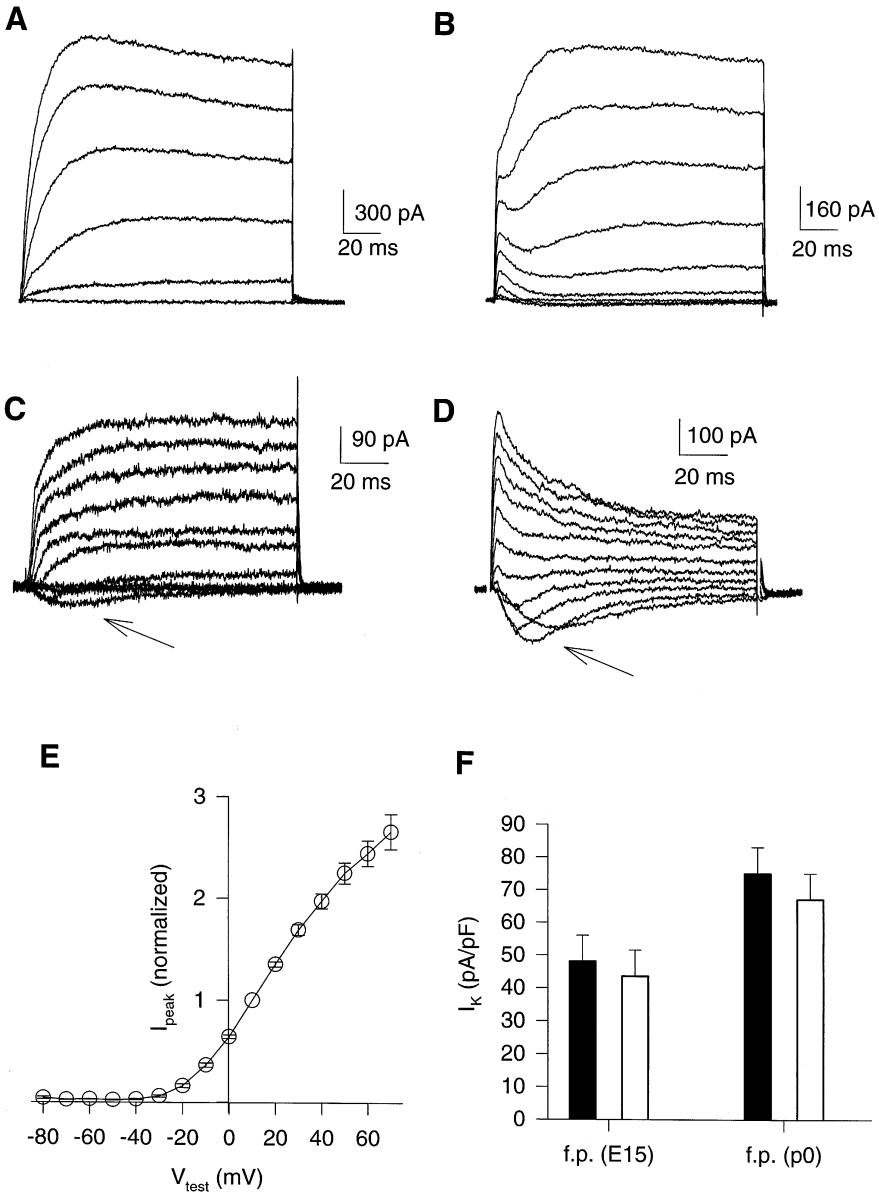

Fig. 2. K^+ conductances produce large ionic currents in neuroepithelial cells. (A) Currents recorded from a P0 floor plate that exhibited only the slowly-activating, slowing-inactivating, outward current. (B) Currents recorded from a neonatal floor plate cell that exhibited both rapidly- and slowly-inactivating outward current components. (C) Example of voltage-activated currents from an embryonic floor plate cell that exhibited only the sustained, slowly-inactivating K^+ current. The arrow indicates the substantial inward current also present in this cell. (D) Currents from an embryonic floor plate cell that possessed both transient and sustained outward K^+ currents. Like the cell in (C), this cell also possessed a substantial voltage-activated inward current (arrow). (E) Peak current–voltage relationships averaged from 30 floor plate neuroepithelial cells recorded under the conditions identical to those in (A). Before averaging each current value was normalized to the current amplitude obtained at +10 mV in the same cell. (F) A bar chart showing the average peak current (filled bars) and sustained current (open bars) recorded at a test potential of +50 mV. Sustained currents were measured as the average current of last 10 ms of a 120 ms test pulse. Data from 14 embryonic floor plate cells (I_{peak}=48 ± 8 pA/pF, I_{sus}=43.5 ± 8 pA/pF) and 30 P0 floor plate cells (I_{peak}=75 ± 8 pA/pF, I_{sus}=67 ± 8 pA/pF). For A to D all currents were generated by depolarizing voltage steps applied from a holding potential of −80 mV. Test pulses were to potentials of −50, −30,…, +50 mV. The largest currents were generated by the largest depolarizations. In all cases, the extracellular solution was standard ACSF and the intracellular solution was ICS1.

t-test) in cells expressing the transient K^+ current (850 ± 210 MΩ) than in those lacking it (360 ± 60 MΩ).

Production of peak current–voltage series from experiments such as those shown in Fig. 2A and 2B revealed that, under these approximately

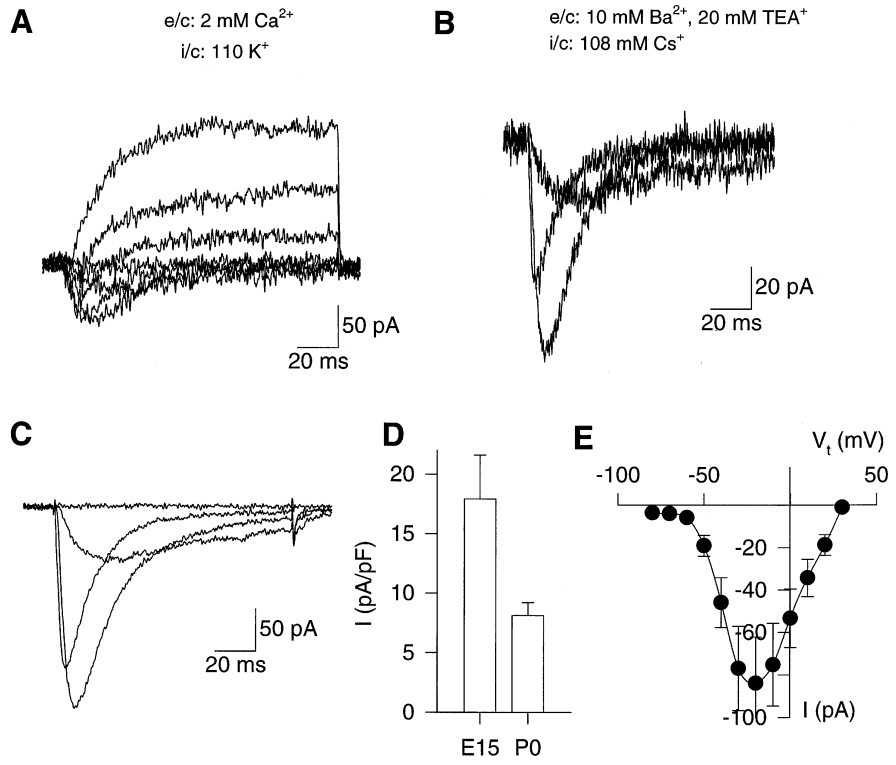

Fig. 3. Isolation of a voltage-activated inward current in floor plate neuroepithelia. (A) Example of current sweeps from a P0 floor plate cell bathed in ACSF and recorded with intracellular ICS1, $V_h = -80$ mV, $V_t = -60, -50, \ldots +10$ mV. Note the small but significant inward currents at the onset of the test pulse. (B) A recording from a different P0 floor plate cell illustrating that a larger and uncontaminated inward current can be observed by making recordings with intracellular ICS2 and by adding 20 mM TEA and 10 mM Ba^{2+} to the perfusing ACSF; $V_h = -80$ mV, $V_t = -40, -20$, and 0 mV. (C) A similar recording to that in B, but in this case from an embryonic floor plate cell. The holding potential was -80 mV and the test potentials $-60, -40, -20$ and 0 mV. (D) The graph plots the averaged peak Ca^{2+} current at -30 mV (normalized to cell capacitance) from nine embryonal and 63 new-born (P0) floor plate cells. Extracellular solution: ACSF plus 20 mM TEA, intracellular solution: ICS2. (E) A graph of the relationship between peak inward current and test potential for 19 neonatal floor plate cells recorded under the conditions shown in B.

physiological conditions (extracellular ACSF and intracellular ICS1), K^+ currents in floor plate cells first exhibited detectable activation near -30 mV (Fig. 2E). We quantified the voltage-dependence of K^+ current activation in neonatal floor plate cells by converting the peak I–V relationship from each cell to the equivalent conductance–voltage relationship. The curves thus produced were then fit with standard first order Boltzmann functions. The mean values of the two free parameters of these fits (see Experimental Procedures) were $V_{1/2} = 2.0 \pm 0.5$ mV and Boltzmann slope factor, $k = 13.7 \pm 0.4$ mV. Quite similar parameter values ($V_{1/2} = 7.4 \pm 1.3$ mV, $k = 13.8 \pm 1.0$ mV) were obtained if currents measured 100 ms after the onset of depolarization were used instead of peak currents to determine conductance.

Peak outward current vs voltage plots from six embryonic cells with relatively smaller contaminating inward currents suggested the voltage-dependence of K^+ current activation in embryos was essentially similar to that of neonates. Figure 2F plots the average, capacitance normalized, peak and sustained K^+ current amplitudes, for embryonic and neonatal floor plate cells, recorded at $V_t = +50$ mV. This indicates that K^+ current densities become greater as floor plate cells age; this was a significant difference ($P < 0.01$, t-test).

As in many other systems, the transient K^+ current could be completely and selectively eliminated by depolarizing the steady-state holding potential of the cell, in this case to -40 mV. Using this technique we were able to subtractively determine the kinetics of the transient K^+ current and thereby compare it to its more prolonged counterpart. The transient K^+ current exhibited faster activation kinetics at all test potentials examined (data not shown). Inactivation of the transient K^+ current component was basically voltage-independent, with a time constant of 12 ± 2 ms at +10 mV. Recovery from inactivation proceeded along a biexponential trajectory best described by time constants of 6.7 ms and 68.2 ms. The faster time constant contributed 38% to the total recovery. Inactivation of the sustained current component was characterized with depolarizations lasting

800 ms. In contrast to the transient K^+ current, the slow inactivation of this current was somewhat voltage-dependent, increasing in rate with stronger depolarization (τ_{inact}=610 ± 185 ms at V_t=−10 mV; τ_{inact}=236 ± 33 ms at V_t=+50 mV).

T-type calcium currents in floor plate cells

The traces shown in Fig. 2C and D indicate that, in addition to K^+ currents, a substantial inward current was present in embryonic floor plate cells. In a few neonatal cells recorded under these near physiological conditions (extracellular ACSF and ICS1), a similar current was discernible in the initial few milliseconds following depolarization to potentials of between −50 and −10 mV. An example of such a cell is shown in Fig. 3A. Under these recording conditions this inward current was always rapidly masked by the rising phase of the much larger outward K^+ current.

In order to investigate this inward current more closely, K^+ currents were eliminated by application of extracellular TEA (20 mM) and use of ICS2 instead of ICS1. In many experiments we also substituted 10 mM $BaCl_2$ for the 2 mM $CaCl_2$ usually present in our standard ACSF. Under these conditions a large well-isolated inactivating inward current could be observed in the test potential range −50 to +30 mV (Fig. 3B). Of 61 neonatal floor plate cells recorded under these conditions 43 clearly possessed this inward current. An inward current of very similar kinetics and voltage dependence was observed in 18 out of 18 embryonic floor plate cells (Fig. 3C). Under all conditions studied, the amplitude of the transient inward current was considerably greater in the floor plate cells of embryonic slices. For instance in 2 mM extracellular Ca^{2+}, the current averaged 17.9 ± 3.7 pA/pF in embryos as compared to 8.1 ± 1.1 pA/pF in neonates (P<0.001 t-test, Fig. 3D).

Data illustrating the mean current–voltage relationships pooled from 19 neonatal floor plate cells, recorded in the presence of 10 mM Ba^{2+}, are shown in Fig. 3E. Net inward currents are clearly active at a test potential of −50 mV and the peak current occurs close to −20 mV. Such behaviour is not commensurate with activation of a high-voltage-activated (HVA) Ca^{2+} current which would be expected to exhibit little or no current until $V_t \geq -30$ mV and would exhibit a peak current near +10 mV, in 10 mM Ba^{2+}. The inward current was completely insensitive to application of 1 μM TTX.

Permeation and block of the calcium current

With HVA Ca^{2+} channels (i.e. L-, N-, P-, Q- and R-type Ca^{2+} channels) and TTX-sensitive Na^+ channels excluded, the main candidates for the conductance(s) underlying the inactivating inward current in floor plate cells are low-voltage-activated (LVA) Ca^{2+} channels and TTX-insensitive Na^+ channels. To separate between these two possibilities, we performed a series of ion substitution and addition experiments. Example data from one such experiment performed on a floor plate cell in the spinal cord of an E15 embryo is shown in Fig. 4A. The graph plots the peak amplitude of the inward current recorded at a test potential of −20 mV versus time. Initially the extracellular solution contained 20 mM TEACl and 2 mM Ca^{2+}; the intracellular solution was ICS2. Under these conditions the inward current amplitude remained stable for 12 min. After this period the bathing solution was exchanged for one containing 10 mM Ba^{2+} in place of 2 mM Ca^{2+}. This caused a 1.8-fold increase in the inward current amplitude. Ni^{2+} (100 μM) was then added to the extracellular solution. This caused an ∼65% depression in the peak current amplitude, an effect which reversed slowly upon washout of Ni^{2+}.

We performed a considerable number of related experiments on the voltage-activated inward current of both neonatal embryonic floor plate cells. Pooled data from selected manipulations are illustrated in Fig. 4B–E. Figure 4B illustrates the average effect of exchanging 2 mM extracellular Ca^{2+} for 10 mM extracellular Ba^{2+}. A very similar increase in peak current was found when increasing the Ba^{2+} concentration from 2 to 10 mM (n=4, data not shown). The potentiation of current amplitude upon increasing the extracellular divalent ion concentration is good evidence that the inward current arises from activation of a Ca^{2+} conductance rather than a Na^+ conductance. Particularly since the test potentials used in these experiments, −20 or −30 mV, were selected to be very close to the peak of the current–voltage relationship (Fig. 3E). This means that the increase in current could not arise from a surface charge screening-induced shift towards the peak of the I–V relationship.

It is possible to make distinctions between different Ca^{2+} channel subtypes by comparing their relative permeabilities to Ca^{2+} and Ba^{2+}. We therefore performed experiments comparing the amplitude of the voltage-activated inward current in solutions containing either 10 mM Ca^{2+} or 10 mM Ba^{2+}. To limit any effects arising from differential surface charge screening by these two ions, we studied currents at potentials close to the peak of the I–V relationship. Pooled time-course data from five such experiments are shown in Fig. 4C. It is clear that the Ca^{2+} channel in floor plate cells is essentially equipermeant to these two ions. This observation strengthens the case that the inward current is carried by the T-type Ca^{2+} channel.

LVA T-type Ca^{2+} channels exhibit a characteristic pattern of sensitivity to the divalent cations Ni^{2+} and Cd^{2+}. We tested the ability of these two ions to block the inward current carried by 10 mM Ba^{2+} in floor plate cells. Ni^{2+} (40–120 μM) caused a robust, dose-dependent and slowly reversible block in all cells tested. The decrease in peak current amplitude was

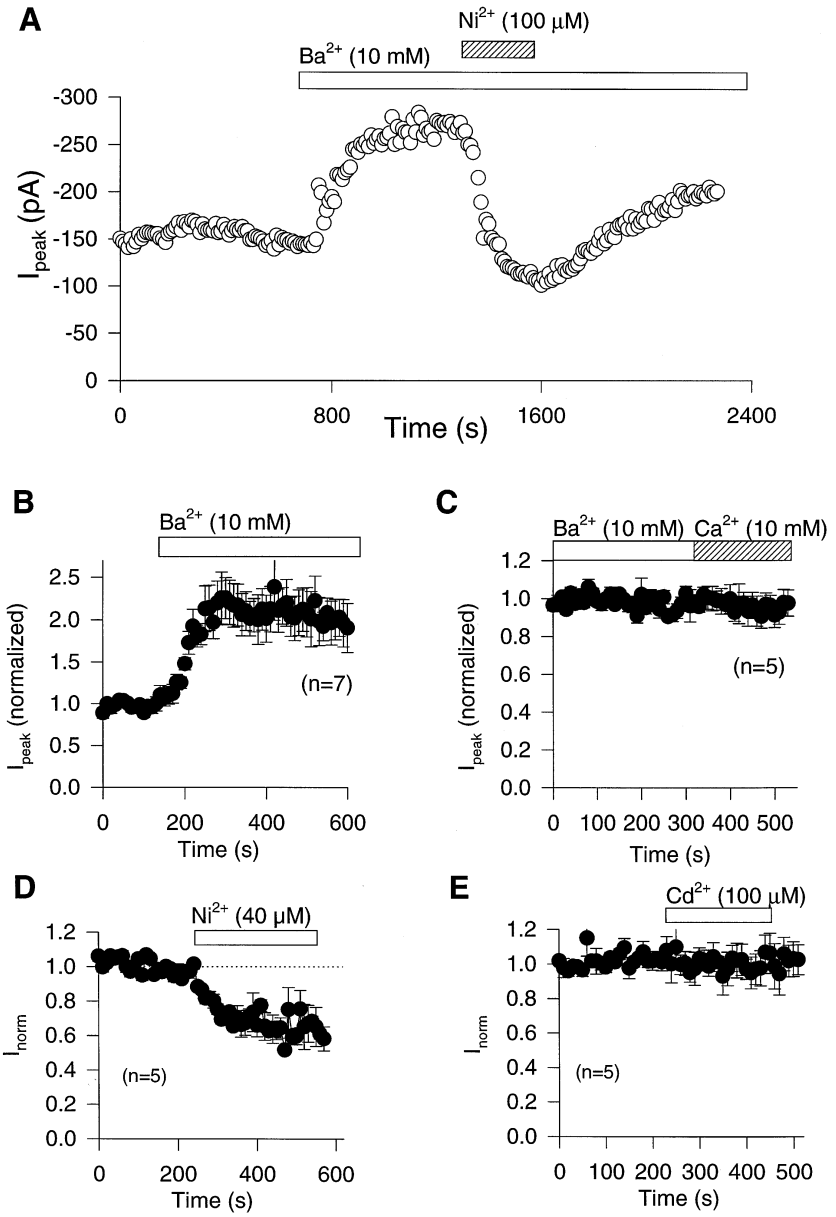

Fig. 4. Permeation and block of the voltage-activated inward current in floor plate neuroepithelia. (A) A graph of peak inward current vs time for an experiment illustrating the potentiation of the inward current in an E15 embryo floor plate cell seen when switching from 2 mM extracellular Ca^{2+} to 10 mM extracellular Ba^{2+} and its subsequent inhibition by Ni^{2+} (100 µM). The holding potential was −80 mV and the test potential was −20 mV. The initial extracellular solution was ACSF plus 20 mM TEA, the intracellular solution was ICS2. (B) A graph plotting data pooled from seven cells and illustrating the average change in inward current amplitude induced by switching the perfusing solution from one containing 2 mM Ca^{2+} to one containing 10 mM Ba^{2+}. Currents were elicited by 40 ms voltage steps from −80 to −30 or −20 mV. Before averaging, data from each cell were normalized to the average amplitude in 2 mM Ca^{2+}. The extracellular solution contained 20 mM TEA, the intracellular solution was ICS2. (C) A graph illustrating that switching the bathing solution from one containing 10 mM Ba^{2+} to one containing 10 mM Ca^{2+} has little or no effect on the inward current amplitude elicited by 40 ms voltage step from −80 to −20 mV. Data from five cells, each normalized to its average response in 10 mM Ba^{2+}. (D) Pooled data from five floor plate cells indicating that application of 40 µM Ni^{2+} blocks the Ba^{2+} current, elicited by a test pulse from −80 to −20 mV, by ~36%. Data from each cell were normalized to average baseline amplitude before averaging. (E) A graph illustrating the effect of the application of Cd^{2+} (100 µM) to five floor plate cells. Current elicited and averaged as in D.

not accompanied by any major change in current waveform. The pooled data presented in Fig. 4D demonstrate that a 5-min application of 40 μM Ni^{2+} blocked the inward current by 36 ± 1% in neonatal floor plate cells. Experiments performed on E15 embryonic floor plate cells (e.g., Fig. 4A) revealed an indistinguishable sensitivity to Ni^{2+} ions.

T-type channels are relatively insensitive to blockade by Cd^{2+} ions, whereas all HVA Ca^{2+} channels, including the Ni^{2+}-sensitive R-type conductance, are blocked by Cd^{2+} with an IC_{50} of ~1 μM. Cd^{2+} ions (40 and 100 μM) were found to be an ineffective blocker of the inward Ca^{2+} current in both neonatal and embryonic floor plate cells. This is illustrated for neonatal cells in Fig. 4E, which plots pooled data on the effect of 100 μM Cd^{2+} on the Ca^{2+} current of five cells. This insensitivity to Cd^{2+} confirms that the Ca^{2+} current is carried almost exclusively by T-type channels.

Activation and inactivation of the Ca^{2+} current

The experiments described above provide good evidence that the inward current present in neonatal and embryonic floor plate cells arises from activation of an LVA T-type Ca^{2+} channel. We characterized the basic activation and inactivation properties of this channel in the presence of 10 mM extracellular Ba^{2+}. Steady-state inactivation curves were generated by varying the holding potential stepwise in 5 mV increments from −80 to −35 mV. The cell was clamped at each holding potential for 10 s before a test pulse to −20 mV was applied. As the holding potential was depolarized, the peak current observed during the test pulse became considerably smaller, until it became undetectable with holding potentials of around −40 mV (Fig. 5A). A graph of pooled steady-state inactivation data from seven such experiments is shown in Fig. 5B (filled symbols). The data could be well fit by a standard Boltzmann function of slope 5.5 mV and 50% inactivation at −57 mV (see Experimental Procedures for function).

The T-type current activation curve recorded in 10 mM extracellular Ba^{2+} is also plotted in Fig. 5B. This curve was derived from the I–V relationship shown in Fig. 3E, using interpolated reversal potentials to calculate conductance. This activation curve could be well fit by a Boltzmann function with a half activation potential of −36 mV and a slope of 7.4 mV. These activation and inactivation characteristics are entirely consistent with LVA (but not HVA) Ca^{2+} channels recorded under similar conditions in other systems. It is notable that there is a significant "window" current present at the overlap of the activation and inactivation curves. Simple calculations suggest that at potentials of −55 to −45 mV, with physiological extracellular Ca^{2+} concentrations, steady Ca^{2+} currents of 2–5 pA and 7–15 pA could be generated in neonatal and embryonic floor plate cells, respectively.

Rapid inactivation during maintained depolarizations is a hallmark of LVA T-type Ca^{2+} channels.[20] Accordingly, the LVA Ca^{2+} current in floor plate cells exhibited rapid inactivation during the course of depolarizing test pulses (e.g., Fig. 3B and C). We analysed the voltage-dependence of the inactivation process by fitting single exponential functions to the decaying phase of the current activated at various test potentials. The rate of inactivation was greatly enhanced at more depolarized levels. A plot of mean inactivation time constant against test potential is shown in Fig. 5E. This graph illustrates that at test potentials of ≥0 mV the inactivation time constant approached an asymptote at ~8 ms. These rates of inactivation are slightly faster than those previously reported for LVA Ca^{2+} channels (τ=15–50 ms at 0 mV) and HVA Ca^{2+} channels (τ=25–500 ms at 0 mV) but are somewhat slower than those usually seen for TTX-insensitive Na^{+} channels (τ≤4 ms at −20 mV).[20,38,66]

Figure 5C illustrates a typical two pulse experiment designed to determine the rate of recovery from inactivation of the T-type current. A plot of fractional recovery against time from 38 such experiments (Fig. 5D) shows that, like T-type currents in other systems, recovery is relatively slow, taking >2 s for total deinactivation to be achieved. On average half-recovery from inactivation was achieved after ~400 ms at −80 mV.

$GABA_A$ receptors in neuroepithelium cells

The experiments described above indicate that floor plate neuroepithelia possess at least two types of K^{+} current as well as a T-type Ca^{2+} channel. The negative voltage range of activation of the T-type channel suggests it could be recruited in resting floor plate cells by quite small depolarizing stimuli. In neurons, such a change in membrane potential would typically be provided by the activation of neurotransmitter receptors at synapses. Synaptically released neurotransmitters have also been reported to depolarize non-neuronal cells in the CNS.[10,31,35] We were, therefore, interested to see if the activation of any such receptors could also generate ionic currents in floor plate cells.

We applied the CNS neurotransmitters GABA, glutamate, glycine and 5-hydroxytryptamine (5-HT) to floor plate cells voltage-clamped at −80 mV. The bath solution was standard ACSF and the electrode was filled with either ICS1 or ICS3. The excitatory neurotransmitter glutamate (100 μM) produced no detectable response in eight of nine floor plate cells tested. 5-HT (100 μM) and glycine (100 μM) were equally ineffective in each of two cells examined (Fig. 6A). All three ligands were without effect irrespective of whether the cells were studied in voltage-clamp or current-clamp.

The inhibitory neurotransmitter GABA (1 mM), in contrast, produced responses in 26 out of 33 floor

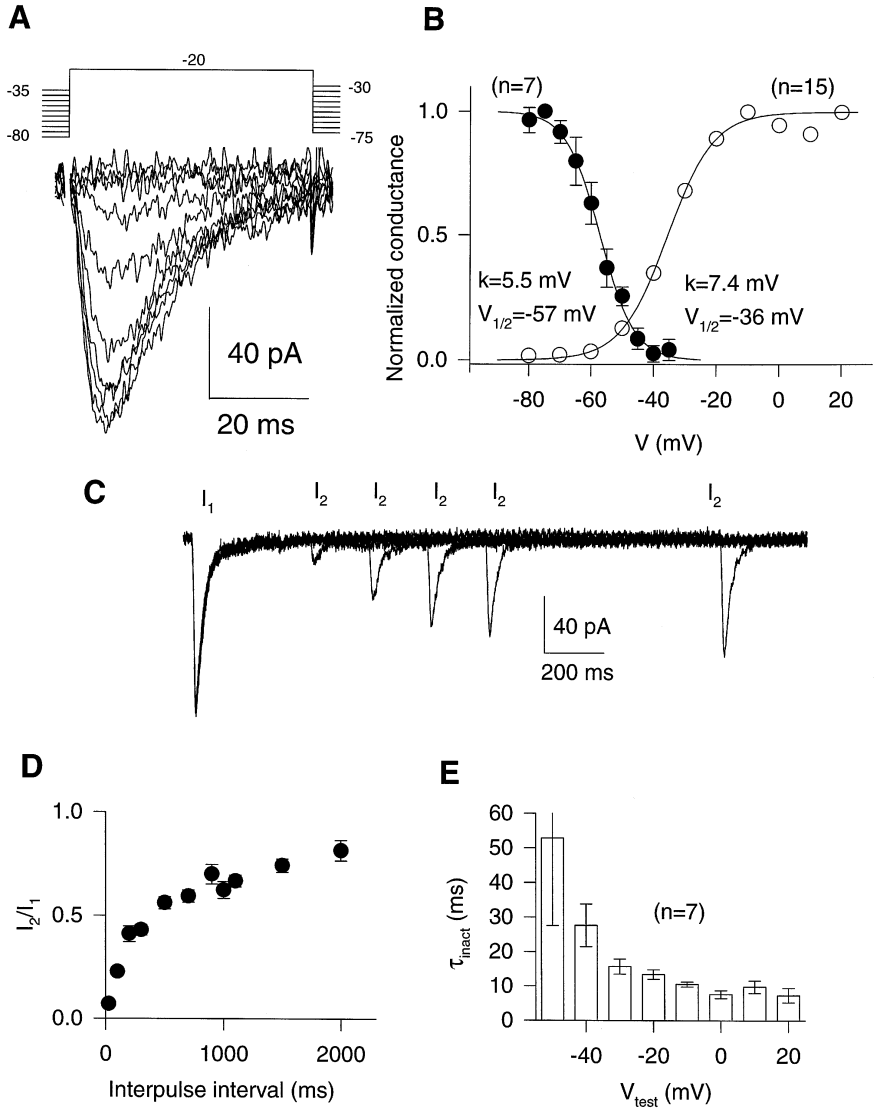

Fig. 5. Activation and inactivation of T-type Ca^{2+} currents in floor plate cells. (A) A standard steady-state inactivation voltage protocol (top) with an example of the current responses generated in a typical cell (bottom). Recordings were carried out in the presence of 10 mM extracellular Ba^{2+}. (B) Plots of average normalized activation (n=15, open symbols) and steady-state inactivation (n=7, filled symbols) experiments. Each data set is fitted with a suitable Boltzmann function. The inactivation data are fitted with a curve of $V_{1/2}=-57.2$ mV and slope 5.5 mV. The activation data are fitted with function of $V_{1/2}=-35.6$ mV and slope 7.4 mV. (C) An example of an experiment where two 300 ms pulses to +20 mV were used to establish the time-course of recovery from inactivation of the Ca^{2+} current in floor plate cells. Interpulse intervals illustrated: 100, 300, 500, 700 and 1500 ms. (D) A graph of the ratio of the peak amplitude of the first and second currents at various interpulse intervals. Data pooled from 32 floor plate cells. (E) Average data from seven floor plate cells illustrating the mean time constant of inactivation plotted against test potential in the range -50 to +20 mV.

plate cells examined. Similar responses were seen in both neonatal and embryonic cells. An example of a voltage-clamp recording from a neonatal floor plate cell voltage-clamped at -80 mV using ICS3 is shown in Fig. 6A. Following ineffectual applications of 5-HT (0.1 mM) and glycine (0.1 mM), GABA (1 mM) was seen to produce a large inward current. In this cell and all other cells examined, marked desensitization of the inward current response occurred during the period of agonist exposure. Upon removal of GABA the current recovered to baseline levels after 6–10 min of washout (data not shown). In cells where two successive applications of GABA were made the second application produced another, typically somewhat smaller, inward current.

The competitive $GABA_A$ receptor antagonist bicuculline methchloride applied at 100 μM completely eliminated responses to 1 mM GABA. Upon washout of bicuculline the GABA response was recovered (data not shown). This suggests that the

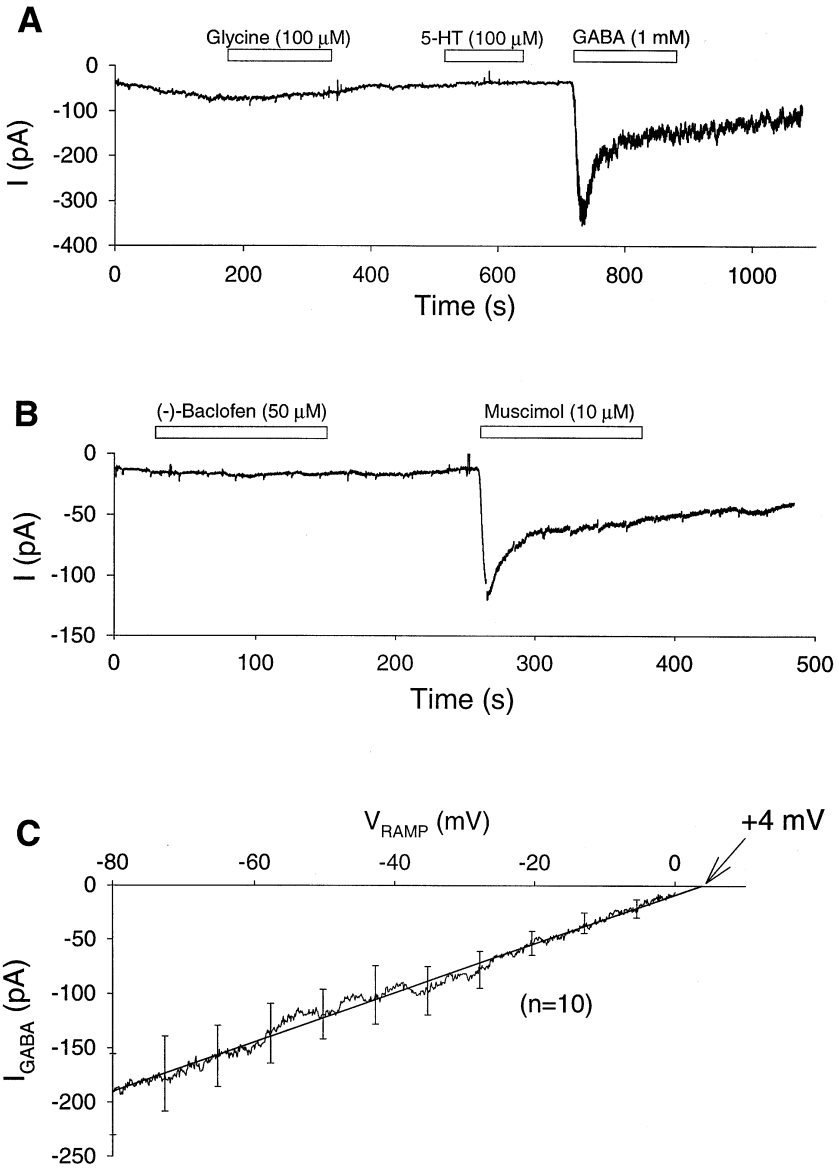

Fig. 6. GABA-induced currents in floor plate cells. A graph of membrane current vs time for a new-born floor plate cell voltage-clamped at a membrane potential of −80 mV. The time of bath applications of 100 μM glycine, 100 μM 5-HT and 1 mM GABA is shown by the open bars. (B) Another cell recorded under the same conditions as that in A illustrating the actions of (−)-baclofen (50 μM) and muscimol (10 μM). In both A and B current deflections resulting from regularly applied voltage ramps have been removed. (C) Pooled data illustrating the voltage-dependence of GABA-induced currents recorded from 10 floor plate cells. The plot illustrates the average of current responses derived from the subtraction of voltage ramp-induced currents recorded before the application of GABA from those recorded after the addition of GABA (1 mM). The graph plots current vs ramp potential. Error bars from the averaging procedure are shown at occasional intervals. A best straight line fit through the data is shown, it intercepts the voltage axis at a potential of +4 mV (arrow).

GABA responses in floor plate cells are mediated by activation of the $GABA_A$ receptor. This was confirmed in experiments like that shown in Fig. 6B. Here the selective $GABA_B$ receptor agonist (−)-baclofen (50 μM) produced no response whereas subsequent application of the selective $GABA_A$ receptor agonist muscimol (10 μM) produced a robust desensitizing inward current. (−)-Baclofen was similarly ineffective, irrespective of holding potential in the range −80 to 0 mV, on four further floor plate cells (three recorded with ICS1 and one with ICS3). Muscimol produced responses in six of 11 floor plate cells.

To further characterize the GABA-mediated response, we recorded the responses to voltage ramps both before and during application of GABA. The ramps were applied every 20 s and depolarized the cell from −80 to 0 mV in 750 ms. By subtracting

the ramp response recorded in the absence of GABA from that recorded near the peak of the GABA response we were able to generate a curve representing the voltage-dependence of the GABA response. Pooled data from 10 such recordings all made using ICS3 are shown in Fig. 6C. This illustrates that the mean inward current produced at −80 mV was about 190 pA and the average extrapolated reversal potential was +4 mV, which when corrected for a 3.4 mV liquid junction potential (see Experimental Procedures) gave a corrected reversal potential value of +0.6 mV, very close to the calculated Cl^- reversal potential of −0.6 mV. In cells recorded with ICS1, the reversal potential shifted in a negative direction, as expected for an intracellular solution containing a lower Cl^- concentration.

DISCUSSION

Similar ion channels are present in embryonic and neonatal in floor cells

The floor plate is a structure that plays an important role in the development of the nervous system. The work presented here is the first study detailing the electrophysiological properties of the neuroepithelial cells that are central to the developmental duties this structure performs. Previous insights into the signalling activities of these cells have relied almost solely upon the methods of biochemistry and cell and molecular biology. It is our belief that electrophysiology, and other related physiological techniques such as Ca^{2+} imaging,[19] also can play a part in understanding how these cells perform their various developmental tasks.

Although remnants of floor plate persist until about P7, the best understood functions of this structure take place in intermediate embryonic stages. Indeed, no clear postnatal function for the floor plate has yet been described. However, for reasons of technical ease, a substantial number of our recordings were carried out on the well-defined floor plate of day of birth rat pups. Recordings from E15 floor plate cells, however, consistently demonstrated the presence of a very similar complement of ion channels, as well identical membrane potentials and capacitances. Indeed, the only obvious differences between neonatal and embryonic floor plate cells were in the amplitude, rather than presence, of any particular current type. For instance, the Ca^{2+} current per unit area of cell membrane was about 2.5-times larger in embryos than in neonates, whereas K^+ currents, in contrast, were somewhat smaller in embryonic cells.

Resting membrane potentials support T-type channel function

Floor plate cells lack TTX-sensitive Na^+ channels and thus cannot generate classical Na^+-dependent action potentials. We also found no evidence for the TTX-resistant fast Na^+ current recently reported in the hypothalamic Y1 neuroepithelial cell line[66] or the TTX-insensitive Na^+ channel reported in dorsal root ganglion cells.[39] Indeed, the only current that could conceivably generate significant depolarizing activity was the T-type Ca^{2+} current, which was found in the large majority of floor plate cells.

When considering if any ion channel is likely to play a role in the function of a particular cell, a resting membrane potential suitable for its activity is prerequisite. In this respect, the resting membrane potential of floor plate cells is ideally poised to allow the T-type channel to gate in response to small depolarizing stimuli. At the median resting membrane potential (−59 mV), approximately 50% of the T-type channels are not inactivated, and are therefore competent to open in response to a depolarizing stimulus. This would lead to: (i) Ca^{2+} influx and (ii) further depolarization of the cell and the recruitment of a greater Ca^{2+} conductance.

Putative excitatory roles for $GABA_A$ receptor activation and axonal K^+ extrusion

Floor plate cells exhibit substantial $GABA_A$ receptor-mediated responses (Fig. 6). Neurons within the floor plate region receive spontaneously active GABAergic and glutamatergic synaptic inputs (AR and FF, unpublished observations). In other systems it has been demonstrated that synaptically-released neurotransmitters, including GABA, can escape the confines of the synapse, thereby producing quite spatially diffuse actions in both neurons and glial cells.[10,24,31,35] Additionally, glial cells in close proximity to axon tracts can be activated by the activity-dependent non-vesicular release of neuroactive substances from the axon.[7] Thus, the possibility exists that GABA released from active neurons could activate the $GABA_A$ receptors of floor plate cells.

It is presently unclear if activation of $GABA_A$ receptors would depolarize or hyperpolarize floor plate cells *in vivo* (our responses always followed the Cl^- gradient imposed by the recording solutions we used). It is noteworthy in this respect that GABA responses in both mature and immature glial cells,[32,59] and in many immature neurons are usually depolarizing in nature (e.g., see Ref. 60). GABA-induced depolarization of floor plate cells would rapidly recruit T-type Ca^{2+} channels, thereby producing rises in intracellular Ca^{2+}. A similar mechanism can be found in the rodent oligodendrocyte-type 2 astrocyte (O-2A) progenitor cells[27] which respond to $GABA_A$ receptor activation with increases in $[Ca^{2+}]_i$. The Cl^- equilibrium potential reported for many immature neurons and glia lays within the narrow voltage range in which significant steady "window" currents through T-type Ca^{2+} channels can be observed (Fig. 5B). Thus constitutive activation of a chloride conductance, such as that of the

$GABA_A$ receptor, could promote prolonged Ca^{2+} entry into floor plate cells.

One somewhat simpler but quite feasible mechanism for activity-dependent depolarization of floor plate cells comes from the fact that K^+ ions can accumulate in the immediate locality of active axons.[40] It is possible that K^+ leakage from active commissural axons crossing the floor plate may depolarize the membrane potential the few millivolts required to activate the T-type Ca^{2+} channel. Through such a mechanism floor plate cells could sense the electrical behaviour of axons in their immediate vicinity.

We detected two separate K^+ channel phenotypes in floor plate neuroepithelial cells. One was present in all floor plate cells examined and was relatively slow to both activate and inactivate. This channel can be regarded as a classical delayed rectifier. A proportion of cells possessed an additional more rapidly-activating and rapidly-inactivating "transient" K^+ current. It is likely that cells with the transient K^+ current will behave somewhat differently from those lacking it, being able to more rapidly and effectively counter depolarizing influences.

Our impression was that cells expressing the transient K^+ current were more commonly found in regions of the floor plate somewhat displaced from the mid-line. Cells with the transient K^+ current exhibited significantly higher resting input impedances than their counterparts with only delayed rectifier K^+ currents, indicating they will depolarize more in response to a given excitatory stimulus. Differential medial-lateral expression of other signalling molecules has previously been reported in the floor plate.[19,34] This has lead to speculation that all floor plate cells are not equal with medial-lateral location possessing some functional importance.[6,19,34,42]

Possible consequences of calcium channel activation in floor plate cells

E16 floor plate cells possess the cellular machinery to produce elevations in intracellular Ca^{2+} via the phosphoinositide pathway.[19] Our work suggests these cells additionally possess the ability to produce voltage-gated changes in intracellular Ca^{2+}. Notwithstanding how they are produced, the cellular consequences of elevations in cytoplasmic Ca^{2+} in floor plate cells are likely to be wide-reaching. Ca^{2+} acts as a multifunctional second messenger regulating practically all cellular processes. Ca^{2+} ions trigger the selective expression of certain genes,[15] and thereby could control both the proliferation and differentiation of floor plate cells during development. Ca^{2+} signals are also likely to trigger changes in the metabolism, morphology and the receptor complement of floor plate cells.

CONCLUSION

From a functional viewpoint, a very interesting possibility is that elevated intracellular Ca^{2+} concentrations in floor plate cells could stimulate the exocytosis. Although not generally implicated in fast synaptic neurotransmitter release, T-type channels have been implicated in the somewhat slower release of aldosterone from the adrenal gland.[1] The presence of growing axons in close proximity to the floor plate has been reported to stimulate the release of chemoattractant/chemorepellant substances.[11] It is attractive to hypothesize that these substances are released in response to elevations in intracellular Ca^{2+}, possibly triggered by $GABA_A$ receptor activation and subsequent T-type Ca^{2+} channel gating.

On a cautionary note, although suggestive of a role in floor plate function, the presence of ion channels in embryonic floor plate neuroepithelia by no means provides strong evidence that these channels play any part whatsoever in diverse developmental functions of the floor plate. Much more experimental work will be required to either disregard or conclusively demonstrate the part played by the T-type Ca^{2+} channel or the $GABA_A$ receptor in floor plate function. Having said this, the data presented here provide a sound basic framework to allow such questions to be addressed in the future. We are currently developing new experimental approaches to investigate these and related questions concerning the functions of ion channels in floor plate cells.

Acknowledgements—This work was supported by the Medical Research Council. We would like to thank Drs S. Hunt and F. Liversey for their advice during the project.

REFERENCES

1. Barret P. Q., Ertel E. A., Smith M. M., Nee J. J. and Cohen C. J. (1995) Voltage gated calcium currents have two opposing effects on the secretion of aldosterone. *Am. J. Physiol.* **268,** 985–992.
2. Bernhardt R. R., Nguyen N. and Kuwada J. Y. (1992) Growth cone guidance by floor plate cells in the spinal cord of zebrafish embryos. *Neuron* **8,** 869–882.
3. Bernhardt R. R., Patel C. K., Wilson S. W. and Kuwada J. Y. (1992) Axonal trajectories and distribution of GABAergic spinal neurons in wildtype and mutant zebrafish lacking floor plate cells. *J. comp. Neurol.* **326,** 263–272.
4. Bovolenta P. and Dodd J. (1990) Guidance of commissural growth cones at the floor plate in embryonic rat spinal cord. *Development* **109,** 435–447.
5. Bovolenta P. and Dodd J. (1991) Perturbation of neuronal differentiation and axon guidance in the spinal cord of mouse embryos lacking a floor plate: analysis of Danforth's short-tail mutation. *Development* **113,** 625–639.

6. Campbell R. M. and Peterson A. C. (1993) Expression of a lacZ transgene reveals floor plate cell morphology and macromolecular transfer to commissural axons. *Development* **119,** 1217–1228.
7. Chiu S. Y. and Kriegler S. (1994) Neurotransmitter-mediated signalling between axons and glial cells. *Glia* **11,** 191–200.
8. Clarke J. D., Holder N., Soffe S. R. and Storm M. J. (1991) Neuroanatomical and functional analysis of neural tube formation in notochordless *Xenopus* embryos; laterality of the ventral spinal cord is lost. *Development* **112,** 499–516.
9. Colamarino S. A. and Tessier-Lavigne M. (1995) The axonal chemoattractant netrin-1 is also a chemorepellent for trochlear motor axons. *Cell* **81,** 621–629.
10. Dani J. W., Chernjavsky A. and Smith S. J. (1992) Neuronal activity triggers Ca^{2+} waves in hippocampal astrocyte networks. *Neuron* **8,** 429–440.
11. DeFelipe C., Pinnock R. D. and Hunt S. P. (1995) Modulation of chemotropism in the developing spinal cord by substance P. *Science* **267,** 899–902.
12. Dodd J. and Jessel T. M. (1988) Axon guidance and the patterning of neuronal projections in vertebrates. *Science* **242,** 692–699.
13. Ericson J., Thor S., Edlund T., Jessell T. M. and Yamada T. (1992) Early stages of motor neuron differentiation revealed by expression of homeobox gene Islet-1. *Science* **256,** 1555–1560.
14. Frischknecht F. and Randall A. D. (1996) *In vitro* electrophysiological recordings from cells in the floor plate region of the new-born rat. *J. Physiol.* **491,** 139P.
15. Ghosh A. and Greenberg M. E. (1995) Calcium signalling in neurones: molecular mechanisms and cellular consequences. *Science* **268,** 239–247.
16. Goulding M. D., Lumsden A. and Gruss P. (1993) Signals from the notochord and floor plate regulate the region-specific expression of two Pax genes in the developing spinal cord. *Development* **117,** 1001–1016.
17. Hatta K. (1992) Role of the floor plate in axonal patterning in the zebrafish CNS. *Neuron* **9,** 629–642.
18. Hatta K., Kimmel C. B., Ho R. K. and Walker C. (1991) The cyclops mutation blocks specification of the floor plate of the zebrafish central nervous system. *Nature* **350,** 339–341.
19. Heath M. J. S., Lints T. J., Lee C. J. and Dodd J. (1995) Functional expression of the tachykinin NK-1 receptor by floor plate cells in the embryonic rat spinal cord and brainstem. *J. Physiol.* **486,** 139–148.
20. Hille B. (1992) *Ionic Channels of Excitable Membranes*. Sinauer, Sunderland.
21. Hirano S., Fuse S. and Sohal G. S. (1991) The effect of the floor plate on pattern and polarity in the developing central nervous system. *Science* **251,** 310–313.
22. Holley J. A. and Silver J. (1987) Growth pattern of pioneering chick spinal cord axons. *Devl Biol.* **123,** 375–388.
23. Hynes M., Poulsen K., Tessier-Lavigne M. and Rosenthal A. (1995) Control of neuronal diversity by the floor plate: contact-mediated induction of midbrain dopaminergic neurons. *Cell* **80,** 95–101.
24. Issacson J. S., Solis J. M. and Nicoll R. A. (1993) Local and diffuse synaptic actions of GABA in the hippocampus. *Neuron* **10,** 165–175.
25. Jessel T. M. and Dodd J. (1990) Floor plate-derived signals and the control of neuronal cell pattern in vertebrates. *Harvey Lect.* **86,** 87–128.
26. Kennedy T. E., Serafini T., de la Torre J. and Tessier-Lavigne M. (1994) Netrins are diffusible chemotropic factors for commissural axons in the embryonic spinal cord. *Cell* **78,** 425–435.
27. Kirchoff F. and Kettenmann H. (1992) GABA triggers a $[Ca^{2+}]_i$ increase in murine precursor cells of the oligodendrocyte lineage. *Eur. J. Neurosci.* **4,** 1049–1058.
28. Klar A., Baldassare M. and Jessell T. M. (1992) F-spondin: a gene expressed at high levels in the floor plate encodes a secreted protein that promotes neural cell adhesion and neurite extension. *Cell* **69,** 95–110.
29. Klar A., Jessell T. M. and Ruiz A. A. (1992) Control of floor plate identity and function in the embryonic nervous system. *Cold Spring Harbor Symp. quant. Biol.* **57,** 473–482.
30. Kuwada J. Y., Bernhardt R. R. and Chitnis A. B. (1990) Pathfinding by identified growth cones in the spinal cord of zebrafish embryos. *J. Neurosci.* **10,** 1299–1308.
31. Linden D. J. (1997) Long-term potentiation of glial synaptic currents in cerebellar culture. *Neuron* **18,** 983–994.
32. MacVicar B. A., Tse F. W. Y., Crackton S. E. and Kettenmann H. (1989) GABA activated Cl^- channels in astrocytes of hippocampal slices. *J. Neurosci.* **9,** 3577–3583.
33. Marti E., Bumcrot D. A., Takada R. and McMahon A. P. (1995) Requirement of 19K form of Sonic hedgehog for induction of distinct ventral cell types in CNS explants. *Nature* **375,** 322–325.
34. McKanna J. and Cohen S. (1989) The EGF receptor kinase substrate p35 in the floor plate of the embryonic rat CNS. *Science* **243,** 1477–1479.
35. Mennerick S., Benz A. and Zorumski C. F. (1996) Components of glial responses to exogenous and synaptic glutamate in rat hippocampal microcultures. *J. Neurosci.* **16,** 55–64.
36. Messersmith E. K., Leonardo E. D., Shatz C. J., Tessier-Lavigne M., Goodman C. S. and Kolodkin A. L. (1995) Semaphorin III can function as a selective chemorepellent to pattern sensory projections in the spinal cord. *Neuron* **14,** 949–959.
37. Muller B. K., Bonhoeffer F. and Drescher U. (1996) Novel gene families involved in neural pathfinding. *Curr. Opin. genet. Dev.* **6,** 469–474.
38. Nargeot J., Clozel J.-P. and Tsien R. W. eds (1997) *T-Type Ca^{2+} Channels*. Adis, Chester (in press).
39. Ogata N. and Tabebayashi H. (1993) Kinetic analysis of two types of Na^+ channels on rat dorsal root ganglia. *J. Physiol.* **466,** 9–37.
40. Orkand R. K., Nicholls J. G. and Kuffler S. W. (1966) Effect of nerve impulses on the membrane potential of glial cells in the central nervous system of amphibia. *J. Neurophysiol.* **29,** 788–806.
41. Placzek M. (1995) The role of the floor plate and notochord in inductive interactions. *Curr. Opin. genet. Dev.* **5,** 499–506.
42. Placzek M., Jessell T. M. and Dodd J. (1993) Induction of floor plate differentiation by contact-dependent, homeogenetic signals. *Development* **117,** 205–218.
43. Placzek M., Tessier-Lavigne M., Yamada T., Jessel T. and Dodd J. (1990) Mesodermal control of neuronal cell identity: floor plate induction by the notocord. *Science* **250,** 985–988.

44. Placzek M., Yamada T., Tessier-Lavigne M., Jessell T. and Dodd J. (1991) Control of dorsoventral pattern in vertebrate neural development: induction and polarizing properties of the floor plate. *Development* **2,** 105–122.
45. Raff M. C. (1996) Neural development: mysterious no more? *Science* **274,** 1063.
46. Roelink H., Porter J. A., Chiang C., Tanabe Y., Chang D. T., Beachy P. A. and Jessell T. M. (1995) Floor plate and motor neuron induction by different concentrations of the amino-terminal cleavage product of sonic hedgehog autoproteolysis. *Cell* **81,** 445–455.
47. Schoenwolf G. C. and Smith J. L. (1990) Mechanisms of neuralation: traditional viewpoints and recent advances. *Development* **109,** 243–270.
48. Serafini T., Kennedy T. E., Galko M. J., Mirzayan C., Jessell T. M. and Tessier-Lavigne M. (1994) The netrins define a family of axon outgrowth-promoting proteins homologous to *C. elegans* UNC-6. *Cell* **78,** 409–424.
49. Shirasaki R., Tamada A., Katsumata R. and Murakami F. (1995) Guidance of cerebellofugal axons in the rat embryo: directed growth toward the floor plate and subsequent elongation along the longitudinal axis. *Neuron* **14,** 961–972.
50. Smith J. L. and Schoenwolf G. C. (1989) Notochordal induction of cell wedging in the chick neural plate and its role in neural tube formation. *J. exp. Zool.* **250,** 49–62.
51. Stoeckli E. T. and Landmesser L. T. (1995) Axonin-1, Nr-CAM, and Ng-CAM play different roles in the *in vivo* guidance of chick commisural neurons. *Neuron* **14,** 1165–1179.
52. Suter D. M., Pollerberg G. E., Buchstaller A., Giger R. J., Dreyer W. J. and Sonderegger P. (1995) Binding between the neural cell adhesion molecules axonin-1 and NrCAM/Bravo is involved in neuron–glia interaction. *J. Cell Biol.* **131,** 1067–1081.
53. Tamada A., Shirasaki R. and Murakami F. (1995) Floor plate chemoattracts crossed axons and chemorepels uncrossed axons in the vertebrate brain. *Neuron* **14,** 1083–1093.
54. Tanabe Y. and Jessel T. M. (1996) Diversity and pattern in the developing spinal cord. *Science* **274,** 1115–1123.
55. Tessier-Lavigne M. and Goodman C. S. (1996) The molecular biology of axon guidance. *Science* **274,** 1123–1133.
56. Tessier-Lavigne M., Placzek M., Lumsden A. G. S., Dodd J. and Jessel T. M. (1988) Chemotrophic guidance of developing axons in the mammalian central nervous system. *Nature* **336,** 775–778.
57. van Straaten H. and Hekking J. W. (1991) Development of floor plate, neurons and axonal outgrowth pattern in the early spinal cord of the notochord-deficient chick embryo. *Anat. Embryol.* **184,** 55–63.
58. van Stratten H. W., Hekking J. W., Wiertz-Hoessels E. J., Thors F. and Drukker J. (1988) Effect of notochord on the differentiation of a floor plate area in the neural tube of the chick embryo. *Anat. Embryol.* **177,** 317–324.
59. von Blankenfeld G., Trotter J. and Kettenmann H. (1991) Expression and developmental regulation of a $GABA_A$ receptor in cultured murine cells of the oligodendrocyte lineage. *Eur. J. Neurosci.* **3,** 310–316.
60. Wang J., Reichling D. B., Kyrozis A. and MacDermott A. B. (1994) Developmental loss of GABA- and glycine-induced depolarization and Ca^{2+} transients in embryonic rat doral horn neurons in culture. *Eur. J. Neurosci.* **6,** 1275–1280.
61. Wright D. E., White F. A., Gerfen R. W., Silos-Santiago I. and Snider W. D. (1995) The guidance molecule semaphorin III is expressed in regions of the spinal cord and periphery avoided by growing sensory axons. *J. comp. Neurol.* **361,** 321–333.
62. Yaginuma H., Homma S., Kunzi R. and Oppenheim R. W. (1991) Pathfinding by growth cones of commissural interneurons in the chick embryo spinal cord: a light and electron microscopic study. *J. comp. Neurol.* **304,** 78–102.
63. Yaginuma H. and Oppenheim R. W. (1991) An experimental analysis of *in vivo* guidance cues used by axons of spinal interneurons in the chick embryo: evidence for chemotropism and related guidance mechanisms. *J. Neurosci.* **11,** 2598–2613.
64. Yamada T., Pfaff S. L., Edlund T. and Jessell T. M. (1993) Control of cell pattern in the neural tube: motor neuron induction by diffusible factors from notochord and floor plate. *Cell* **73,** 673–686.
65. Yamada T., Placzek M., Tanaka H., Dodd J. and Jessell T. M. (1991) Control of cell pattern in the developing nervous system: polarizing activity of the floor plate and notochord. *Cell* **64,** 635–647.
66. Zhang X., Phelan K. D. and Geller H. M. (1996) A novel tetrodotoxin resistant sodium current from an immortalized neuroepithelial cell line. *J. Physiol.* **490,** 17–29.

(*Accepted* 24 *November* 1997)